Journal of Materials Chemistry

Cite this: *J. Mater. Chem.*, 2011, **21**, 8835

www.rsc.org/materials

PAPER

Effects of titania nanotube distance and arrangement during focused ion beam guided anodization

Bo Chen, Kathy Lu* and Zhipeng Tian

Received 12th March 2011, Accepted 14th April 2011
DOI: 10.1039/c1jm11083g

Anodic TiO_2 nanotube arrays possess exciting application potentials in solar cells and photocatalysis. However, self-organized anodization alone can only produce randomly arranged nanotubes. In this study, focused ion beam (FIB) guided anodization is used to create highly ordered TiO_2 nanotube arrays with different intertube distances and tube arrangements. On the one hand, FIB patterning greatly enhances the organization of the nanotubes for the classic hexagonal close packing. On the other hand, fundamentally different nanotube arrangements, such as square, oblique hexagonal, and alternating-sized patterns, are also created. The self-compensating effect enables the development of alternating-sized TiO_2 nanotube hexagonal arrays from graphite lattice FIB guiding patterns. The mechanism of the FIB guided anodization is proposed. This approach presents great opportunities in producing ordered TiO_2 nanotubes and new nanotube arrangements for the desired applications.

1. Introduction

TiO_2 has attracted much interest in recent years due to its excellent photocatalytic activity.[1] It has been applied to photocatalysts,[2,3] water photoelectrolysis,[4,5] light induced superhydrophilic/super-hydrophobic surfaces,[6,7] dye-sensitized solar cells,[8–12] and sensors.[13,14] TiO_2 nanotubes are one of the most desired morphologies because of their large surface area, well controlled size, and added novel properties from different tube sizes and alignments. They offer excellent electron percolation pathways and large internal surface areas to improve the charge collection efficiency by facilitating electron transport and reducing electron–hole recombination in dye-sensitized solar cells. The enhanced optical absorption due to light-scattering effect and the transparent property of TiO_2 nanotube film further increase the efficiency of dye-sensitized solar cells.

Anodization is one of the most common methods to generate TiO_2 nanotubes from Ti substrates. Self-ordered TiO_2 nanotubes were obtained about two decades ago by anodizing Ti in a fluoride-containing electrolyte.[15] Since then, anodic TiO_2 nanotubes have been obtained from many different electrolytes, such as acid-based electrolyte,[16,17] ethylene/fluoride electrolyte,[18,19] and glycerol/fluoride electrolyte.[20,21] Water content in an electrolyte has a significant effect on the tube diameter, and higher water content leads to larger tube diameter.[22,23] The nanotube diameters (outer diameter) have been varied from 20 to 600 nm[23–25] and the nanotube length can be controlled from <1 μm[26] to >100 μm.[27,28] However, because the TiO_2 nanotubes are generally less than ideal hexagonal packing, the intertube distance has not been well quantified. In addition, most of the anodization work starts from as-received Ti foils without any surface treatment. Our recent work has shown that different surface polishing conditions lead to very different nanotube sizes and morphologies.[29] For two-step anodization, concave arrays are created on titanium surface by peeling off the first nanotube layer, and then used to guide the growth of the next TiO_2 nanotube layer.[30,31] This strategy has improved the TiO_2 nanotube arrangement in some local regions, but the overall anodic nanotube layer still has much to be desired. As a comparison, several methods have been developed to create well-arranged nanopores on Al substrates under guided anodization, such as nano-imprint lithography,[32–34] holographic lithography,[35] and focused ion beam guided anodization.[36–41] It is unknown whether similar guided anodization approaches can be successfully applied to Ti anodization to obtain highly ordered TiO_2 nanotube arrays. More desirably, multiple tube sizes in desired arrangements may be possible and should be explored.

In this study, FIB patterning is used to guide the anodization of Ti foils. Hexagonal, square, oblique hexagonal, alternating-sized hexagonal, and graphite lattice structure guiding patterns are created by FIB on electropolished Ti foils before the anodization. The FIB guidance effect and the influence of interpore distance are examined. Both symmetrical and asymmetrical FIB guiding patterns are explored. The self-compensating effect for missing sites is also explored for the anodization. The TiO_2 nanotube formation mechanism for the FIB guided anodization is discussed.

2. Experimental section

Ti foils (Goodfellow Corporation, Oakdale, PA) with 0.2 mm thickness and 99.6+% purity were first cut to 2.0 cm × 2 mm in

Department of Materials Science and Engineering, Virginia Tech, Virginia, 24061, USA. E-mail: klu@vt.edu; Fax: +1 540 231 8919; Tel: +1 540 231 3225

size, and then cleaned in acetone, isopropanol, and methanol with ultrasonic agitation for 10 min each. After that, electropolishing was carried out in freezing electrolyte (~1 °C) with 800 rpm stirring speed for 2 min under a constant applied potential of 55 V. The electropolishing electrolyte was composed of glacial acetic acid (99.5%, ACROS Organics, Morris Plains, NJ) and perchloric acid (62%, Alfa Aesar, Ward Hill, MA) with a volume ratio of 9 : 1.

The surface roughness of the electropolished Ti surface was further decreased to ~1 nm by the FIB exposure at 28 pA under 30 kV acceleration voltage for 30 s (FEI Helios 600 NanoLab, Hillsboro, OR). The guiding patterns for the anodization were then created on the Ti surface by the FIB bombardment at 28 pA under 30 kV acceleration voltage.[38] Hexagonal, square, oblique hexagonal, alternating-sized hexagonal, graphite lattice structure patterns with different interpore distances were created. By adjusting the total FIB patterning time, the ion exposure time at each patterned concave was 90 ms. The depth of the FIB patterned concaves was measured by the atomic force microscope (Digital Instruments MultiMode SPM, Veeco Instruments Inc., Camarillo, CA).

The anodization was carried out in a two-electrode electrochemical cell in ethylene glycol electrolyte containing 0.1 M NH_4F and 10 vol% DI water at room temperature. The anodization was under 15 mA cm^{-2} constant current density and the voltage saturated at 88 V within 30 s. The constant current density anodization was beneficial for the anodized TiO_2 nanotubes to grow slowly and develop into well-ordered arrays. Then, the anodization was under 88 V constant potential for 5 min with negligible current density deviation from 15 mA cm^{-2}. In order to observe the backside of the TiO_2 nanotubes, the anodized TiO_2 foil was ultrasonicated in 1 : 9 volume ratio of DI water/ethanol for 1 min, then immersed in 0.1 M HCl for 1 h. These processes increased the defects between TiO_2 nanotube bottoms and Ti foil and enabled the detachment of TiO_2 nanotube arrays.[42,43] After rinsing with DI water and drying in nitrogen stream, the anodic TiO_2 nanotube layer was easily peeled off by a tape. The top surface and backside morphologies of the anodized samples were examined using a scanning electron microscope (SEM, Quanta 600 FEG, FEI Company, Hillsboro, OR).

3. Results and discussion

3.1. Highly ordered hexagonal TiO_2 nanotube arrays

FIB patterned concave arrays in hexagonal arrangement with five different interpore distances (d_{inter}) are used to guide the anodization: 150 nm, 200 nm, 300 nm, 400 nm, and 500 nm. Fig. 1a shows a typical FIB patterned hexagonal array on the Ti foil with 300 nm interpore distance. The diameters are 50 nm and the depths are 40 nm for all the FIB patterned concaves (Fig. 1a, inset). The periodicity of the pores is excellent. Fig. 1b–f demonstrate the anodic TiO_2 nanotube arrays under the guidance of the hexagonal FIB patterns with different d_{inter}. After the anodization, a thin layer of ordered nanopore arrays develops at the FIB patterned positions. The backside and cross-section views of the anodic TiO_2 in the insets of Fig. 1 show that the nanopores grow into separated TiO_2 nanotubes. The depths of the TiO_2 nanotube arrays are ~1.3 μm.

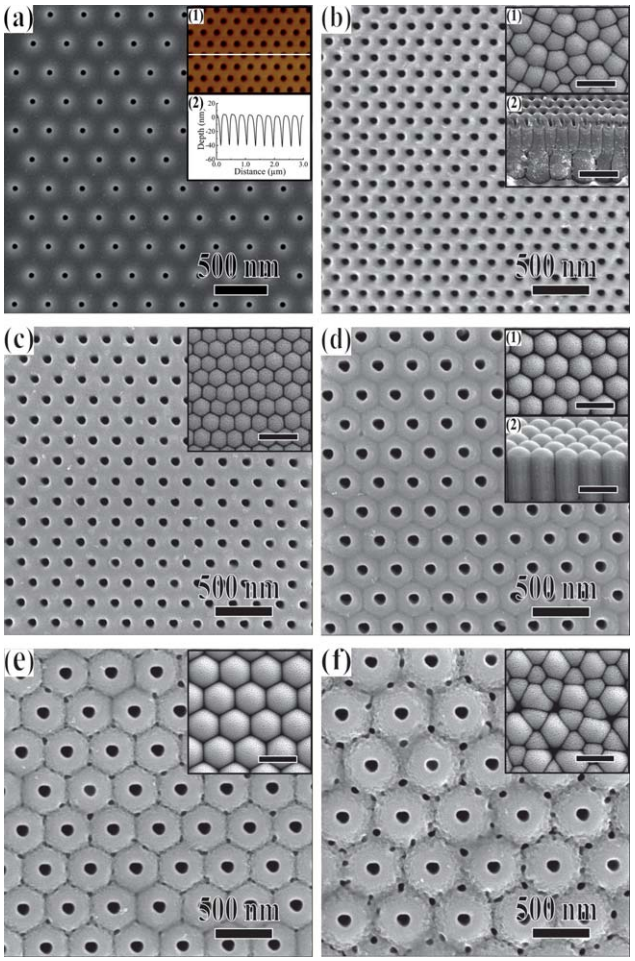

Fig. 1 (a) FIB guiding pattern in hexagonal arrangement with 300 nm interpore distance. The inset (1) is the AFM image of (a) and the inset (2) is the surface topology along the line in inset (1). Anodized TiO_2 nanotube arrays under the guidance of hexagonal FIB pattern with different d_{inter}: (b) 150 nm, (c) 200 nm, (d) 300 nm, (e) 400 nm, and (f) 500 nm. The first insets in b–f are the backside view of the anodic TiO_2 nanotube arrays. The inset (2) in (b) and (d) is the cross-section of the anodized TiO_2 nanotubes. The scale bars in all the insets are 500 nm.

When d_{inter} of the FIB guiding pattern is 150 nm, all the TiO_2 nanotubes grow at the FIB patterned concaves, thus the anodized TiO_2 surface has ordered nanotube arrays (Fig. 1b). However, with further growth, some nanotubes have enlarged outer diameters while some nanotubes terminate as shown in the middle point of the cross-section (inset (2) in Fig. 1b). As a result, the anodized TiO_2 arrays have disordered arrangement at the tube bottoms with outer sizes ranging from 200–300 nm (inset (1) in Fig. 1b). The tube outer wall shape is irregular polygon.

When d_{inter} is 200 nm, the bottom view shows that all the tubes maintain the hexagonal arrangement with slight outer size variation (Fig. 1c). The tube outer wall shows hexagonal shape and the sizes are 180–220 nm. When d_{inter} is further increased to 300 nm and 400 nm, both the anodized surfaces and the tube bottoms show highly ordered TiO_2 nanotube arrays with uniform sizes and ordered hexagonal arrangement (Fig. 1d and e). The tube outer wall shows ideally hexagonal shape. The top surface SEM images in Fig. 1d and e also show hexagonal outer wall boundaries of the nanotubes. The tube bottom images in the insets of Fig. 1d and e

show the outer sizes are around 300 nm and 400 nm, respectively, which are the same as the d_{inter} of the FIB guiding patterns. The freestanding nanotubes are closely bound together, and the spaces between the tubes are very small. This demonstrates the exceptional capability of FIB patterning in guiding ordered TiO_2 nanotube growth. When $d_{inter} = 400$ nm, some new concaves form at the tri-junctions of the FIB guided nanotubes on the top surface (Fig. 1e). However, these concaves terminate at the very surface and do not develop into new tubes. This is because the outer walls of the neighboring FIB guided nanotubes are close to each other, and there is no extra space left to develop new tubes.

When d_{inter} is increased to 500 nm, anodic TiO_2 nanotubes develop not only at the FIB patterned sites but also at the tri-junctions of the FIB patterned concaves (Fig. 1f). The newly formed tubes distribute randomly at the tri-junctions. The large d_{inter} allows the FIB guided TiO_2 nanotubes to fully expand the outer walls into circular shapes on the top surface. The nanotube bottoms in the inset of Fig. 1f indicate that the shapes of these newly developed tube walls are triangular, and the sizes are smaller than those of the FIB guided tubes. Moreover, due to the growth of these new tubes, the outer wall shapes of the FIB guided tubes also change into rhombus or pentagon, and the sizes of the FIB guided tubes decrease from 440 nm to 350 nm.

The development of FIB pattern guided anodization can be understood as follows. At the beginning of the anodization, the surface of Ti is covered entirely with a dense and uniform anodic TiO_2, since active metal Ti is oxidized instantly at ambient condition. The distribution of the electrical field in the TiO_2 layer, however, is strongly correlated with the surface morphological fluctuations (more pronounced fluctuations lead to more localized electrical field). During the growth of TiO_2 nanotube arrays, Ti is oxidized into Ti^{4+} at the metal–oxide interface and migrates outwards under the applied electrical field. Meanwhile, O^{2-} ions are incorporated in the oxide layer and migrate towards the metal–oxide interface. The TiO_2 layer forms due to the interaction of the Ti^{4+} ions with the O^{2-} ions in the electrolyte. The overall reactions for anodic oxidation of Ti can be expressed as:[44,45]

$$Ti + 2H_2O \rightarrow TiO_2 + 4H^+ + 4e^- \quad (1)$$

At the same time, the TiO_2 barrier layer dissolves under the reaction:[44,45]

$$TiO_2 + 6F^- + 4H^+ \rightarrow TiF_6^{2-} + 2H_2O \quad (2)$$

The two reactions reach a balance at steady state anodization and the nanotubes grow deeper into the Ti substrate.

At the beginning of the anodization, the TiO_2 layer is thin and the electric field is large, thus the rate of oxidization is much faster than the rate of dissolution. The TiO_2 layer grows both at the walls and bottom of the FIB patterned pores. However, the expansion of the tube outer walls is restricted by the neighboring pores. The neighboring tube outer walls expand towards each other until they merge into a thicker wall.[46] As a result, the thickness of the oxide layer at the tube wall is much larger than that at the pore bottom. In addition, due to the existence of the initial FIB patterned concaves on the Ti surface, the local electrical field is significantly increased at the bottoms of the patterned concaves. The field-enhanced TiO_2 chemical dissolution preferentially takes place at the concave bottoms.[46,47] The FIB patterned pores serve as the seeds to guide the growth of TiO_2 nanotubes. The tubes grow deeper with the downward movement of the TiO_2 layer at the FIB patterned concave bottoms. The Ga^+ implantation and Ti amorphization during the FIB bombardment also facilitate the growth of the nanotubes at the FIB patterned sites, partly by creating easier ion diffusion paths. With the progression of the anodization, the F^- ions are able to enter the growing TiO_2 lattice because of their small size and be transported through the oxide under the applied electric field (competing with O^{2-}) to the metal–oxide interface by forming water-soluble TiF_6^{2-} complexes.[25] The larger electrical field at the FIB patterned concaves not only concentrates F^- ions at the tube bottoms to enhance the tube growth rate, but also accelerates the migration of the small radius F^- ions towards the metal–oxide interface. Because F^- moves faster than O^{2-}, a significant amount of F^- ions is present at the tube outer wall boundaries, facilitating the dissolution of the boundaries. As a result, separated TiO_2 nanotube arrays are obtained. The chemical dissolution of TiO_2 occurs over the entire length. The TiO_2 tubes grow under the competition between TiO_2 formation and TiF_6^{2-} dissolution. The separation of the TiO_2 nanotubes occurs due to the mechanical weakness of the F^- rich layer where the tube outer walls meet.[25]

Even though the FIB patterned concaves can effectively guide the growth of the TiO_2 nanotubes in the beginning of the anodization, whether the highly ordered hexagonal nanotube arrays can maintain the arrangement in the depth direction is related to the applied potential. In general, the voltage drop across the electrolyte is very small[23,45,48] and the outer diameter of self-organized TiO_2 nanotubes can be described by $D = 2f_{growth}U$,[24,25] where f_{growth} is the growth factor for anodic oxides, 2.5 nm V^{-1} for TiO_2, and U is the applied potential. This is the case when the TiO_2 tubes are apart from each other, the growth of TiO_2 tubes does not influence the neighboring tubes, and the shape of the tubes is circular. For the anodization condition here, the applied potential is 88 V, thus $D = 2 \times 2.5$ nm $V^{-1} \times 88$ V $= 440$ nm.

When the d_{inter} of the FIB guiding pattern is 150 nm, much smaller than D of 440 nm, there is strong competition between the closely arranged nanotubes for outer wall growth, and the large volume expansion stress (volume expansion from Ti to TiO_2 is the Pilling Bedworth ratio of 1.95)[49,50] enlarges the diameter of some tubes through terminating the neighboring tubes. As a result, the hexagonal nanotube arrangement cannot be maintained and changes into disordered tube arrays. When d_{inter} is increased to 200 nm, the competition of the volume expansion of the TiO_2 tubes decreases but still influences the pattern development. The hexagonal arrangement is maintained but with slight difference in tube outer sizes. When d_{inter} is further increased to 300 nm and 400 nm, the volume expansion stress between neighboring TiO_2 tubes is small. Consequently, the anodized TiO_2 nanotube arrays maintain the highly ordered hexagonal arrangement. Due to the confinement of the neighboring tubes, a tube stops expanding its outer diameter once meeting the neighboring tube walls, and the outer wall shape is hexagonal. In the case of $d_{inter} = 500$ nm ($>D$ of 440 nm), even when the tubes fully expand into circular shapes, there is still

enough space ($2 \times 500/3^{1/2} - 440 = 137$ nm) left at the tri-junctions of the FIB patterned concaves to develop new tubes. Furthermore, the development of the new tubes changes the nanotube arrangement and d_{inter} at the tube bottoms, which confines the diameter of the FIB guided tubes.

3.2. Ordered TiO_2 nanotube arrays with square arrangement

Traditional one-step or two-step anodization at best only creates hexagonally arranged TiO_2 nanotube arrays. For the FIB guided anodization, formation of new nanotube patterns becomes possible. Fig. 2a shows a typical FIB patterned square concave array with 300 nm interpore distance, 50 nm diameter, and 40 nm depth. Fig. 2b–f show the anodic TiO_2 nanotube arrays under the guidance of the square FIB patterns with different d_{inter} (150 nm, 200 nm, 300 nm, 350 nm, and 400 nm) after 5 min anodization.

At the beginning of the anodization, ordered nanotubes with square arrangement form due to the square FIB pattern guidance. However, further development of the anodized tubes is related to the interpore distance. When d_{inter} (150 nm) < D (440 nm), the tubes are close to each other, the large volume expansion stress from the neighboring tubes makes some tubes terminate and some tubes expand, thus the square arrangement changes into disordered arrangement with tube outer sizes ranging 180–280 nm. When d_{inter} is 200 nm, the volume expansion stress from the neighboring tubes is reduced, and the square arrangement remains unchanged. However, the tube sizes are still not uniform because of the competition of the volume expansion from neighboring tubes (Fig. 2c). When d_{inter} is further increased to 300 nm and 350 nm, as discussed above, the volume expansion stress between neighboring tubes is small. The tubes expand equally and thus highly ordered TiO_2 nanotube arrays with square arrangement and square outer wall shape are obtained as shown in Fig. 2d and e. At 350 nm intertube distance, some shallow pores form at the quadral-junctions of the patterned concaves. However, these new pores terminate and do not develop into new tubes (Fig. 2e). When d_{inter} is 400 nm, the diagonal of the square is $400 \times 2^{1/2} = 566$ nm and much larger than D (440 nm), the TiO_2 nanotubes expand into more circular shapes on the top surface, the un-anodized region at the quadral-junctions is approximately $400 \times 2^{1/2} - 440 = 126$ nm in size. New tubes form at the quadral-junctions with sizes smaller than the FIB guided tubes (210 nm *vs.* 340 nm). Also, the guided nanotubes evolve into more circular shapes while the new tubes have almost ideal rhombus shapes. As a result, TiO_2 nanotube arrays with square arrangement and alternating sizes are fabricated (Fig. 2f).

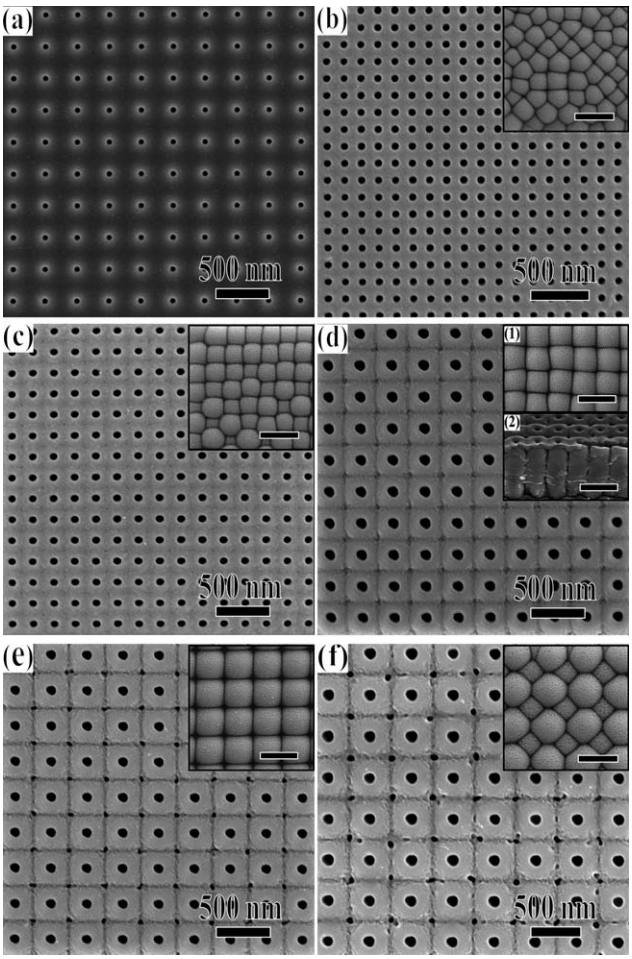

Fig. 2 (a) FIB guiding pattern in square arrangement with 300 nm interpore distance. Anodic TiO_2 nanotube arrays with different intertube distances: (b) 150 nm, (c) 200 nm, (d) 300 nm, (e) 350 nm, and (f) 400 nm. The first insets in all the images are the backside view of the anodic TiO_2 nanotube arrays. The inset (2) in (d) is the cross-section of the tubes. The scale bars in all the insets are 500 nm.

From Fig. 1 and 2, it can be seen that new tubes start to form at 500 nm interpore distance for hexagonal guiding pattern while at 400 nm interpore distance for square guiding pattern. A similar phenomenon for anodic alumina nanopores has been observed and discussed in the previous work.[40] The fundamental reason for this difference is that a hexagonal pattern is more compact than a square pattern in 2D at the same interpore distance. All the tubes in a hexagonal arrangement have the same distance from their neighboring tubes. For a square arrangement, however, the intertube distance in the diagonal direction is larger. Since the guiding effect from the FIB patterned tubes has the same effective range at the same anodization voltage, the square arrangement leaves more room for new tubes to form. As a result, new tubes appear at smaller interpore distance for square guiding patterns.

3.3. Ordered TiO_2 nanotube arrays with more sophisticated arrangements

In this study, not only the guidance of symmetrical FIB patterns (such as hexagonal and square structures) on anodic TiO_2 nanotube formation is examined, but also the guidance of asymmetrical FIB patterns is explored.

Fig. 3a shows FIB patterned concave arrays with oblique hexagonal arrangement. There are three different interpore distances for the neighboring concaves: 200 nm, 250 nm, and 300 nm as shown in the inset of Fig. 3a. All the interpore distances are smaller than that of the free expanding TiO_2 nanotubes (440 nm). The diameters of all the FIB patterned concaves are 50 nm, and the corresponding depths are 40 nm. After the anodization, ordered nanopore arrays are developed on the top surface, and the arrangement stays unchanged (Fig. 3b). The backside view of the anodic TiO_2 in the inset of Fig. 3b shows that the freestanding

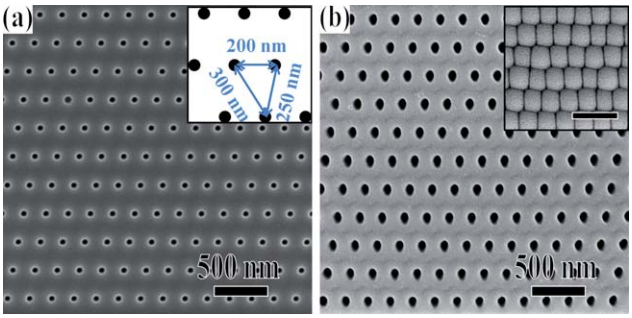

Fig. 3 (a) FIB guiding pattern with asymmetrical arrangement and three different interpore distances: 200 nm, 250 nm, and 300 nm. The inset in (a) is the schematic of different interpore distances. (b) Anodic TiO_2 nanotube arrays after the anodization. The inset in (b) is the backside view of the anodic TiO_2 nanotube arrays, and the scale bar is 500 nm.

TiO_2 nanotubes are closely bound with each other. The shape of the tube bottoms is parallelogram, and the arrangement of the tube array remains oblique hexagonal. The center distances of the three neighboring tube bottoms remain at 200 nm, 250 nm, and 300 nm, respectively. However, if the three interpore distances of the oblique hexagon are decreased to 150 nm, 200 nm, and 250 nm, respectively, the anodized TiO_2 nanotube array cannot maintain the oblique hexagonal arrangement but changes into disordered distribution. As discussed above for the hexagonal patterns, the intertube distance from 200 nm to 400 nm is suitable for maintaining regular arrangements during the anodization; for the square patterns, the intertube distance from 200 to 350 nm can maintain the square arrangements. Fig. 3 shows that even for asymmetrical nanopore arrangement, nanotube arrays with intertube distance ranging from 200 nm to 300 nm can be formed under the guidance of the FIB patterned concaves.

Another sophisticated pattern studied here is hexagonal arrangement with alternating-sized FIB concaves. The diameter of the small concaves is 50 nm, and the diameter of the large concaves is 100 nm (Fig. 4a). The interpore distance is 250 nm. After the anodization, the top surface SEM image (Fig. 4b) shows the anodic TiO_2 nanotubes have almost the same inner diameter at ~65 nm, with the larger tubes showing a crater around the tubes. The backside view of the TiO_2 nanotube arrays indicates that the tubes developed from the large FIB concaves have larger outer dimension (330 nm) and hexagonal shape, while the small tubes developed from the small FIB concaves have elongated hexagonal shape with the long axis at 265 nm and the short axis at 170 nm. The larger size and more regular hexagonal shape of the larger tubes are believed to result from the larger diameter, more Ga^+ implantation, and titanium amorphization of the larger FIB concaves, which makes the corresponding nanotubes grow faster and experience less constraint from the neighboring tube volume expansion, and thus have thicker oxide walls. The small concaves have four small concaves and two large concaves as neighbors to start with. The oxide layer growth in the direction connecting the large tubes is restricted, thus the oxide layer is thinner than that in the direction perpendicular to the connecting line of the large tubes. As a result, the small concaves grow into small tubes with elongated hexagonal shapes.

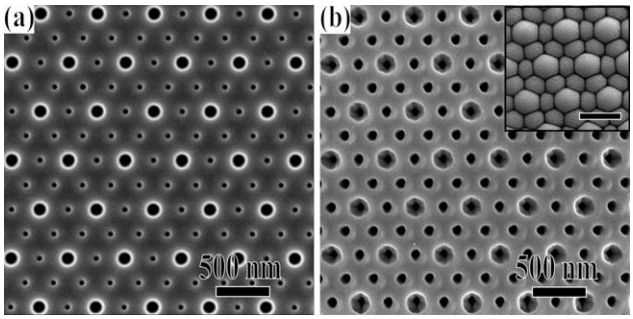

Fig. 4 (a) FIB guiding pattern in hexagonal arrangement with alternating concave diameters, the interpore distance is 250 nm, and the diameters are 50 nm and 100 nm, respectively. (b) Anodic TiO_2 nanotube arrays after the anodization. The inset in (b) is the backside view of the anodic TiO_2 nanotube arrays, and the scale bar is 500 nm.

3.4 Self-compensating effect

The self-compensating effect of anodic TiO_2 nanotubes is another interesting finding for FIB guided anodization. A concave array with graphite lattice arrangement is created by the FIB patterning (Fig. 5a). The interpore distance for neighboring concaves is 250 nm, with 50 nm concave diameter and 40 nm depth. After the anodization, the TiO_2 nanotubes not only grow at the FIB patterned concaves, but also at the centers of the graphite lattice structure due to the self-compensating effect. As a result, hexagonal arrangement of TiO_2 nanotubes with alternating sizes is obtained even though the FIB guiding concaves are purposely designed with missing sites in the hexagonal pattern center (Fig. 5b). The cross-section shows the development and vertical growth of the patterned and new tubes with alternating tube outer wall sizes (inset (2) in Fig. 5b). The fundamental reason can still be traced back to the constraining effect of the oxide layers. For the current pattern design, the distance from each concave to the center of the graphite lattice structure is 250 nm, which is larger than $D/2 = f_{growth}U = 220$ nm. After the oxide layer fully expands in the direction of graphite lattice structure center, there is still enough space left for new tubes to develop at the centers of graphite lattice structure. However, other locations are effectively prevented from the anodization by the oxide layers. Moreover, due to the confinement of the FIB guided nanotubes, the size of the

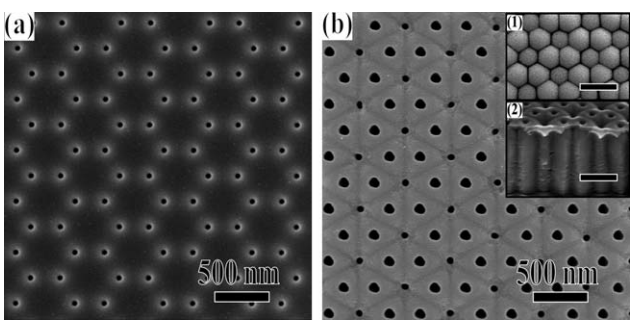

Fig. 5 (a) FIB guiding pattern in graphite lattice arrangement with 250 nm interpore distance. (b) SEM image of TiO_2 nanotube arrays after the anodization. The inset (1) and inset (2) are the backside view and cross-section of the TiO_2 nanotube arrays, respectively. The scale bars in all insets are 500 nm.

newly formed nanotubes is smaller than that of the FIB guided nanotubes, while the hexagonal shape is maintained for both tube sizes. The self-compensation phenomenon, which tolerates the existence of missing concaves for the FIB patterning, is an important advancement in fabricating highly ordered and alternating-sized hexagonal TiO_2 nanotubes.

Conclusions

TiO_2 nanotube arrays with highly ordered hexagonal and square arrangements are created by the FIB guided anodization. The intertube distance for ordered hexagonal arrangement ranges from 200 nm to 400 nm, while for square arrangement it ranges from 200 nm to 350 nm. When the intertube distance is below the guiding range, the anodized tubes initially grow at the locations of the FIB patterned concaves. However, some tubes terminate while other tubes grow larger, and the arrangement changes into disordered when the anodization continues. When the intertube distance is increased above the guiding range, new tubes develop at the junctions of the FIB patterned concaves. More sophisticated TiO_2 nanotube arrays, such as oblique and alternating-sized hexagonal patterns, have been successfully created by the FIB guided anodization. Missing sites from the graphite lattice structure guiding pattern can be self-compensated during the anodization to form ordered hexagonal TiO_2 nanotube arrays with alternating-sized diameters. This study shows the feasibility of fabricating well-ordered TiO_2 nanotubes with the guidance of FIB patterns on the electropolished titanium surface. For the future work, specifically designed FIB equipment can be explored to produce large area FIB patterns with low cost. The anodization process is not limited in sample size or quantity. When this is done, the application potentials of TiO_2 nanotube arrays for nano-devices will be greatly expanded.

Acknowledgements

We acknowledge the financial support from National Science Foundation under grant No. CMMI-0824741 and the Institute of Critical Technology and Applied Science of Virginia Tech (ICTAS). We thank the great help from Dr Yanxi Li, Dr Menghui Li, and Dr Wenwei Ge.

References

1 A. Fujishima and K. Honda, *Nature*, 1972, **238**, 37.
2 S. P. Albu, A. Ghicov, J. M. Macak, R. Hahn and P. Schmuki, *Nano Lett.*, 2007, **7**, 1286.
3 J. M. Macak, M. Zlamal, J. Krysa and P. Schmuki, *Small*, 2007, **3**, 300.
4 G. K. Mor, K. Shankar, M. Paulose, O. K. Varghese and C. A. Grimes, *Nano Lett.*, 2005, **5**, 191.
5 J. H. Park, S. Kim and A. J. Bard, *Nano Lett.*, 2006, **6**, 24.
6 E. Balaur, J. M. Macak, L. Taveira and P. Schmuki, *Electrochem. Commun.*, 2005, **7**, 1066.
7 E. Balaur, J. M. Macak, H. Tsuchiya and P. Schmuki, *J. Mater. Chem.*, 2005, **15**, 4488.
8 K. Zhu, N. R. Neale, A. Miedaner and A. J. Frank, *Nano Lett.*, 2007, **7**, 69.
9 D. Kuang, J. Brillet, P. Chen, M. Takata, S. Uchida, H. Miura, K. Sumioka, S. M. Zakeeruddin and M. Grätzel, *ACS Nano*, 2008, **2**, 1113.
10 O. K. Varghese, M. Paulose and C. A. Grimes, *Nat. Nanotechnol.*, 2009, **4**, 592.
11 J. R. Jennings, A. Ghicov., L. M. Peter, P. Schmuki and A. B. Walker, *J. Am. Chem. Soc.*, 2008, **130**, 13364.
12 C. J. Lin, W. Y. Yu and S. H. Chien, *J. Mater. Chem.*, 2010, **20**, 1073.
13 Q. Zheng, B. X. Zhou, J. Bai, L. H. Li, Z. J. Jin, J. L. Zhang, J. H. Li, Y. B. Liu, W. M. Cai and X. Y. Zhu, *Adv. Mater.*, 2008, **20**, 1044.
14 Y. H. Zhang, P. Xiao, X. Y. Zhou, D. W. Liu, B. B. García and G. Z. Cao, *J. Mater. Chem.*, 2009, **19**, 948.
15 V. Zwilling, E. Darque-Ceretti, A. Boutry-Forveille, D. David, M. Y. Perrin and M. Aucouturier, *Surf. Interface Anal.*, 1999, **27**, 629.
16 A. Ghicov, J. M. Macak, H. Tsuchiya, J. Kunze, V. Haeublein, L. Frey and P. Schmuki, *Nano Lett.*, 2006, **6**, 1080.
17 G. K. Mor, K. Shankar, M. Paulose, O. K. Varghese and C. A. Grimes, *Nano Lett.*, 2006, **6**, 215.
18 H. E. Prakasam, K. Shankar, M. Paulose, O. K. Varghese and C. A. Grimes, *J. Phys. Chem. C*, 2007, **111**, 7235.
19 J. M. Macak and P. Schmuki, *Electrochim. Acta*, 2006, **52**, 1258.
20 A. Valota, D. J. LeClere, T. Hashimoto, P. Skeldon, G. E. Thompson, S. Berger, J. Kunze and P. Schmuki, *Nanotechnology*, 2008, **19**, 355701.
21 J. M. Macak, H. Tsuchiya, L. Taveira, S. Aldabergerova and P. Schmuki, *Angew. Chem., Int. Ed.*, 2005, **44**, 7463.
22 H. Yin, H. Liu and W. Z. Shen, *Nanotechnology*, 2010, **21**, 035601.
23 S. Berger, J. Kunze, P. Schmuki, A. T. Valota, D. J. LeClere, P. Skeldon and G. E. Thompson, *J. Electrochem. Soc.*, 2010, **157**, C18.
24 A. Ghicov and P. Schmuki, *Chem. Commun.*, 2009, (20), 2791.
25 J. M. Macak, H. Hildebrand, U. Marten-Jahns and P. Schmuki, *J. Electroanal. Chem.*, 2008, **621**, 254.
26 S. Bauer, S. Kleber and P. Schmuki, *Electrochem. Commun.*, 2006, **8**, 1321.
27 M. Paulose, K. Shankar, S. Yoriya, H. E. Prakasam, O. K. Varghese, G. K. Mor, T. J. LaTempa, A. Fitzgerald and C. A. Grimes, *J. Phys. Chem. B*, 2008, **112**, 15261.
28 K. Shankar, G. K. Mor, H. E. Prakasam, S. Yoriya, M. Paulose, O. K. Varghese and C. A. Grimes, *Nanotechnology*, 2007, **18**, 065707.
29 Z. P. Tian, J. A. Geldmeier and K. Lu, *Electrochim. Acta*, 2011, accepted.
30 Y. Shin and S. Lee, *Nano Lett.*, 2008, **8**, 3171.
31 S. Q. Li, G. M. Zhang, D. Z. Guo, L. G. Yu and W. Zhang, *J. Phys. Chem. C*, 2009, **113**, 12759.
32 W. Lee, R. Ji, C. A. Ross, U. Gösele and K. Nielsch, *Small*, 2006, **2**, 978.
33 H. Masuda, H. Asoh, M. Watanabe, K. Nishio, M. Nakao and T. Tamamura, *Adv. Mater.*, 2001, **13**, 189.
34 H. Masuda, M. Yotsuya, M. Asano and K. Nishio, *Appl. Phys. Lett.*, 2001, **78**, 826.
35 Z. J. Sun and H. K. Kim, *Appl. Phys. Lett.*, 2002, **81**, 3458.
36 N. W. Liu, A. Datta, C. Y. Liu, C. Y. Peng, H. H. Wang and Y. L. Wang, *Adv. Mater.*, 2005, **17**, 222.
37 P. Schmuki, L. E. Erickson and D. J. Lockwood, *Phys. Rev. Lett.*, 1998, **80**, 4060.
38 C. Y. Liu, A. Datta and Y. L. Wang, *Appl. Phys. Lett.*, 2001, **78**, 120.
39 C. Y. Liu, A. Datta, N. W. Liu, C. Y. Peng and Y. L. Wang, *Appl. Phys. Lett.*, 2004, **84**, 2509.
40 Z. P. Tian, K. Lu and B. Chen, *Nanotechnology*, 2010, **21**, 405301.
41 B. Chen, K. Lu and Z. P. Tian, *Langmuir*, 2011, **27**, 800.
42 Q. W. Chen, D. S. Xu, Z. Y. Wu and Z. F. Liu, *Nanotechnology*, 2008, **19**, 365708.
43 J. H. Park, T. W. Lee and M. G. Kang, *Chem. Commun.*, 2008, (25), 2867.
44 K. Yasuda, J. M. Macak, S. Berger, A. Ghicov and P. Schmuki, *J. Electrochem. Soc.*, 2007, **154**, C472.
45 S. Yoriya and C. A. Grimes, *J. Mater. Chem.*, 2011, **21**, 102.
46 Z. X. Su, G. Hahner and W. Z. Zhou, *J. Mater. Chem.*, 2008, **18**, 5787.
47 J. Choi, R. B. Wehrspohnb and U. Gösele, *Electrochim. Acta*, 2005, **50**, 2591.
48 L. Sun, S. Zhang, X. W. Sun, X. Wang and Y. Cai, *Langmuir*, 2010, **26**, 18424.
49 J. Wang and Z. Q. Lin, *J. Phys. Chem. C*, 2009, **113**, 4026.
50 S. Berger, J. M. Macak, J. Kunze and P. Schmuki, *Electrochem. Solid-State Lett.*, 2008, **11**, C37.

